DISCLAIMER

ORNL/TM-2025/4358

Position-Dependent Neutron Time-of-Flight Deviation at VULCAN Diffractometer

Yan Chen
Dunji Yu
Ke An

December 2025

OAK RIDGE National Laboratory

ORNL IS MANAGED BY UT-BATTELLE LLC FOR THE US DEPARTMENT OF ENERGY

ORNL/TM-2025/4358

Neutron Scattering Division

POSITION-DEPENDENT NEUTRON TIME-OF-FLIGHT DEVIATION AT VULCAN DIFFRACTOMETER

Author(s)

Yan Chen
Dunji Yu
Ke An

December 2025

Prepared by
OAK RIDGE NATIONAL LABORATORY
Oak Ridge, TN 37831
managed by
UT-BATTELLE LLC
for the
US DEPARTMENT OF ENERGY
under contract DE-AC05-00OR22725

This page is intentionally left blank.

CONTENTS

CONTENTS III

LIST OF FIGURES III

ABBREVIATIONS IV

ABSTRACT 1

1. INTRODUCTION 1

2. EXPERIMENT 1

3. RESULTS 3

3.1 STATISTICAL CHANGES IN THE SI CALIBRANT VERSUS PEAK INTENSITY COUNTS 3
3.2 MEASURED DEVIATION IN X-Y PLANE FROM DIFFERENT BANKS 4
3.3 MEASURED DEVIATION IN X-Y PLANE FROM DIFFERENT HKL PLANES 8
3.4 MEASURED DEVIATION IN X-Y PLANE WITH DIFFERENT HORIZONTAL SLIT OPENINGS 10
3.5 MEASURED DEVIATION IN X-Z PLANE WITH DIFFERENT HORIZONTAL SLIT OPENINGS 15

4. SUMMARY 17

REFERENCE 18

ACKNOWLEDGEMENT 19

LIST OF FIGURES

Figure 1. A diamond powder in a Kapton tube was used to scan the beam. 2
Figure 2. Diamond powder diffraction data in Bank 1, the measurement time is 0.5 minutes, and the vertical slit is 12 mm. 2
Figure 3. Relative *d*-spacing fitting error in terms of lattice strain versus peak counts. a) 90^{o} bank, and b) 150^{o} high angle bank. 3
Figure 4. *d*-spacings deviation from the 4-hour-long measurement reference *d*-spacing in terms of microstrain versus peak counts. a) 90^{o} bank, and b) 150^{o} high angle bank. 4
Figure 5. Relative standard deviation from the chopped sub runs, a) 90^{o} bank, and b) 150^{o} high angle bank. 4
Figure 6. Measured deviation in terms of microstrain of (111) in different banks under different guide settings. 5
Figure 7.. Zoomed-in of Fig. 6 with effective sample area marked. 6
Figure 8. Measured deviation in terms of microstrain of (311) in different banks under different guide settings. 7
Figure 9. Zoomed-in of Fig. 8 with effective sample area marked. 8
Figure 10. Tof deviations in terms of microstrain of different hkls in Bank 1. 9
Figure 11. Deviation in terms of microstrain in X-Y plane with different IHA slit openings. 14
Figure 12. Deviation in terms of microstrain in X-Z plane with different horizonal slit openings. 17

ABBREVIATIONS

ORNL	Oak Ridge National Laboratory
SNS	Spallation Neutron Source
FTS	First Target Station
TOF	Time of Flight
HI	High Intensity
HIG9	High Intensity with Guide 9
HRG9	High Resolution with Guide 9

ABSTRACT

In neutron diffraction, it is critical to precisely measure the lattice spacing, as it is an indicator of a material's physical characteristics, such as lattice strain, thermal expansion, and phase structures. In time-of-flight (TOF) measurements, the lattice spacing is determined by the recorded TOF from a well-calibrated instrument. However, changes in neutron time-of-flight are sensitive to many factors, such as the alignment of instrument optics, temperature, sample positions, sample dimensions, internal strains, and chemical or physical heterogeneities at the grain level. At VULCAN (SNS, ORNL), which is a high-flux engineering neutron diffractometer, we used a 1-mm-diameter diamond powder sample to scan for changes in TOF by measuring d-spacing values at different sample positions under several configurations. The 2D map of the TOF deviation or d-spacing deviation, in terms of lattice shift/lattice strain, is reported. The change in TOF is dependent on the scanned location in the beam as well as on detector locations. The results are informative for experimental planning, data interpretation, and future instrument design.

1. Introduction

The VULCAN instrument [1] at the SNS, ORNL, is a diffractometer located on beamline 7 of FTS. It is designed to tackle scientific and engineering problem under external stimuli and probing internal microstructural characteristics non-destructively in structures, such as residual stress, texture, and phases. The incident beam is focused to provide high flux at the sample position, and incident slits are adapted to change incident beam size; along with receiving radial collimators, a gauge volume is defined. The schematic is shown in Fig. 1 from reference [2]. This optics exclude scattering or background from outside the gauge volume, and the changes in the lattice due to external stimuli, such as force or temperature are measured. When measuring residual strains in a structure, the sample can move around the defined gauge volume so that a 2D or 3D strain scan can be achieved. The measured diffraction is a bulk average within the gauge volume. Its resolution depends on the size of the gauge volume, optics, and measurement time. Within the gauge volume, white beam neutron flux is not uniform, thanks to the characteristics of the instrument's guide system, and the TOF is position-sensitive because total path length changes, and even a small change could impact measurement accuracy, which leads to experimental artifacts. It is thus critical to understand the factors that impact diffraction measurements. Here, we used a small diamond powder pin sample, and measured its diffraction patterns by scanning it through the beam with different guide settings. The results are analyzed by fitting different Bragg peaks, and a 2D map of the lattice changes in terms of lattice shift/lattice strain is reported. This report includes all the measured conditions and serves as a reference book on the instrument's measurement performance for different beam configurations.

2. Experiment

Clean corrected version: A 1-mm-diameter diamond powder sample was prepared by filling diamond powder into a Kapton tube. The sample was placed vertically on the instrument stage, as shown in Fig. 1. Different scan grids were used for different instrument settings, with a step size of 1 mm in all scan directions (i.e., X, Y, and Z). A 30 Hz chopper setting was used, with a central wavelength of 2.0 Å and a bandwidth of 2.88 Å. The measurement time was set to 0.5 to 1.5 neutron times, depending on the guide settings. All three available guide settings were used, i.e., high-resolution + Guide 9 [3] (HRG9), high-intensity (HI), and high-intensity + Guide 9 (HIG9). The scans were performed without radial collimators. A typical diffraction pattern of the diamond powder is shown in Fig. 2.

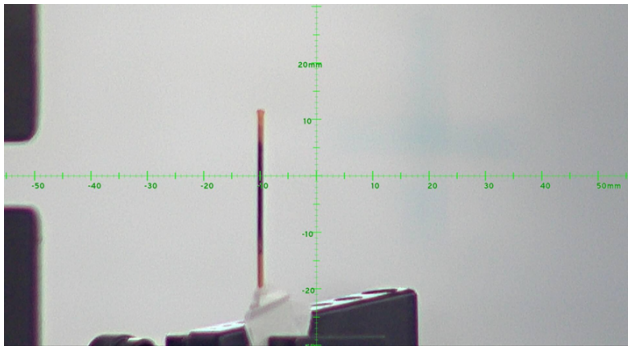

Figure 1. A diamond powder in a Kapton tube was used to scan the beam.

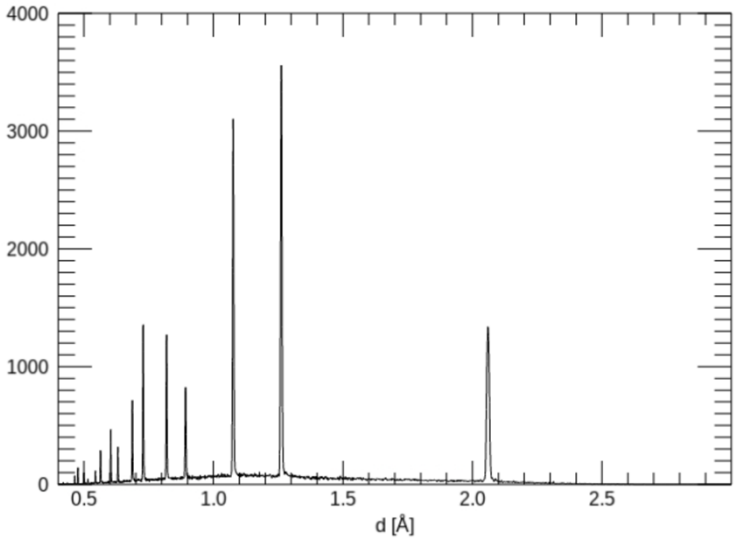

Figure 2. Diamond powder diffraction data in Bank 1, the measurement time is 0.5 minutes, and the vertical slit is 12 mm.

We also investigated changes in fitting errors as a function of peak intensity counts using a Si standard powder in a 6-mm-diameter V can. The incident beam was set to 5 x 10 mm^2, and 5 mm radial collimators were used. The Si sample was measured for 4 hours using a standard 20 Hz chopper setting under HI mode. The data were chopped into various time intervals, and the fitting was performed on several hkls using VDRIVE [4]. The Si data were chopped into: 0.5 min x 480; 1 min x 240; 2 min x 120; 5 min x 48; 10 min x 24; 20 min x 12; 30 min x 8; 60 min x 4; 120 min x 2; and the whole 4-hour measurement. The changes in relative fitting error, relative d-spacing deviation, and relative standard deviation versus peak intensity counts were analyzed.

3. Results

3.1 Statistical changes in the Si calibrant versus peak intensity counts

The fitting error of d-spacing is deduced from the covariance of a single-peak fit in GSAS [5]. In GSAS, the intensity-versus-time-of-flight data is fitted using profile function number 3. It outputs the peak position and fitting error in TOF. The d-spacing is calculated from the quadratic relation between TOF and lattice d-spacing:

$$Tof = DIFC \cdot d + DIFA \cdot d^2 + ZERO \quad (1)$$

The unit of TOF is μs (microseconds); d is the lattice d-spacing in Å, and therefore the units of the quadratic coefficients $DIFC$, $DIFA$, and $ZERO$ are μs/Å, μs/Å^2, and μs, respectively. The relative fitting error is defined as the ratio of the fitting error (d_{err}) in d-spacing to the corresponding d-spacing. We use microstrain as the unit by multiplying the relative fitting error by 10^6. Since the data were chopped into different numbers of runs for a given total count, we used the average value of the fitted d-spacing (d_{ave}) and the average fitting error ($d_{err,ave}$). Fig. 3 shows the relative d-spacing fitting error in terms of microstrain versus peak intensity counts. The data collected in the 90° bank and the 150° bank are presented here. Overall, the relative fitting error decreases with increasing peak intensity counts, and it continues to decrease, although the rate of decrease diminishes with increasing peak intensity counts. The fitting error can go below 100 microstrain at approximately 1000 counts in the 90° bank, whereas the relative fitting error in the high-angle 150° bank is much smaller. The hkl dependence is less pronounced with increasing counts and converges for most of the measured peaks, except for Si (111).

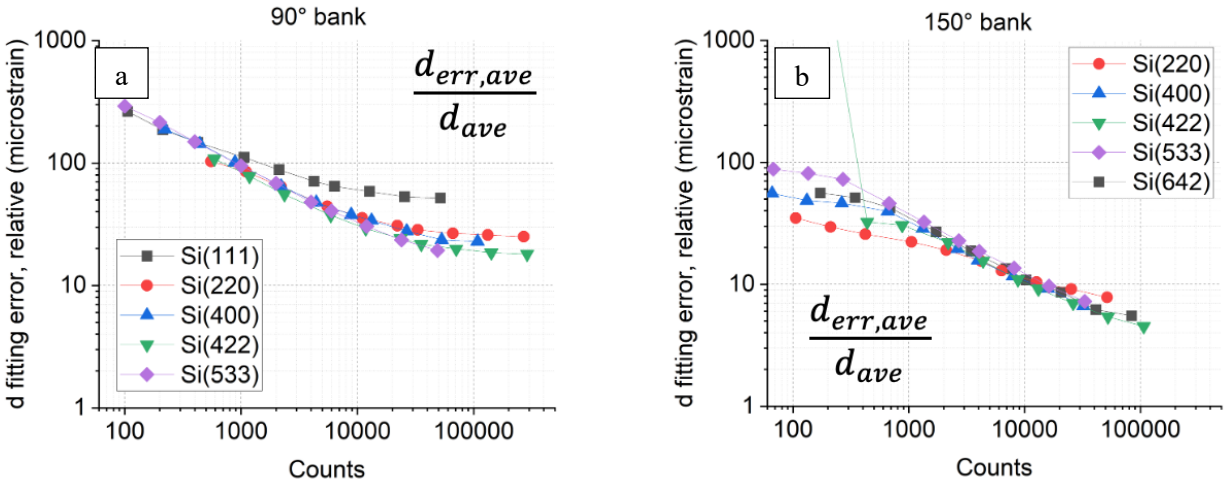

Figure 3. Relative d-spacing fitting error in terms of lattice strain versus peak counts. a) 90° bank, and b) 150° high angle bank.

Taking the 4-hour long measurement as the reference, d deviation (same as the Tof deviation), or d-spacing average difference from chopped sub runs are presented in microstrain, were calculated by (d_{ave}/d-1) x10^6, and they are plotted as a function of peak intensity counts. The results are presented in Fig. 4. From the reduced data in both banks, the greater the counts or the longer the counting time, the smaller the deviation is. The values are small, on the order of a few microstrain, and approach 0 quickly. Statistically, the average standard deviation represents the accuracy of the measurement. Its dependence on peak intensity counts is plotted in Fig. 5. The data follow a linear relationship after taking logarithmic scales for both the relative standard deviation and the peak intensity counts. To study the location-dependent time-of-flight shift, the Si data provide guidance on how long we can obtain reliable data points without overcounting neutrons. Considering the strong scattering power of diamond powder, the planned times of 0.5 to 1.5 neutron minutes are sufficient for good peak fitting, and the effect of counting statistics on the scanned results can be neglected, so the position-dependent TOF deviation can be explored using the diamond powder scan.

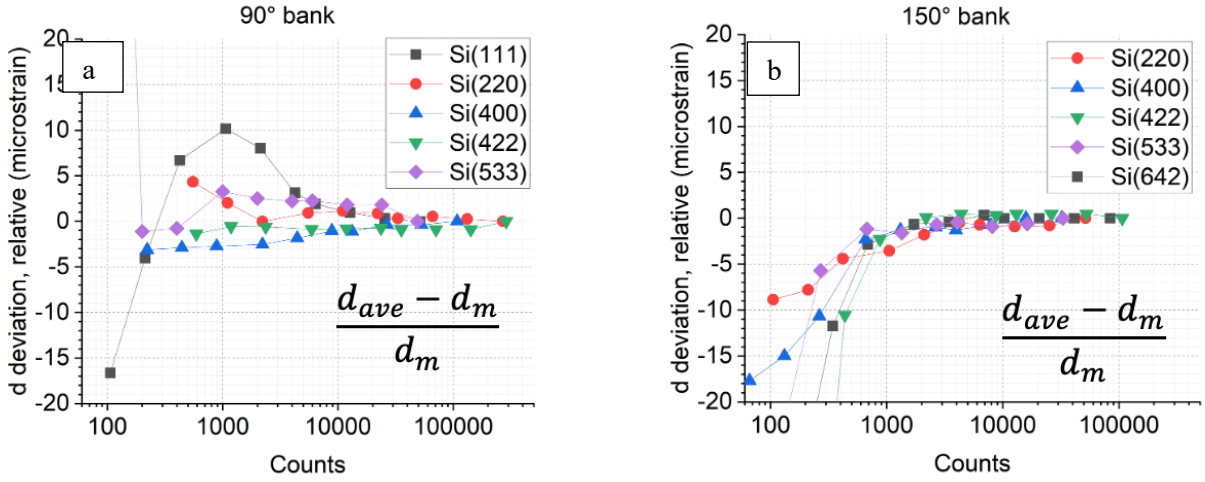

Figure 4. *d*-spacings deviation from the 4-hour-long measurement reference *d*-spacing in terms of microstrain versus peak counts. a) 90° bank, and b) 150° high angle bank.

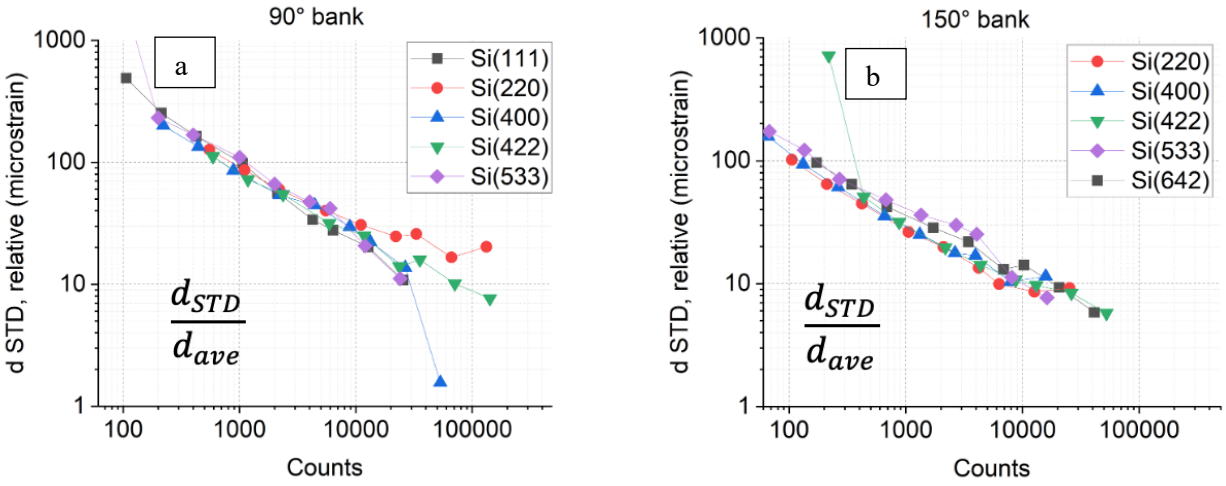

Figure 5. Relative standard deviation from the chopped sub runs, a) 90° bank, and b) 150° high angle bank.

3.2 Measured deviation in X-Y plane from different banks

We first investigated d-spacing deviation in different banks by using different guides. The (111) peak was used and single peak fitting was done. In Fig. 6, the scanned lattice d-spacing changes in XY plane with X being the incident beam direction are shown in bank 1, bank 2 and bank 6. As mentioned above, the guide settings are HIG9, HI, and HRG9. The incident slits are set as 12x12 mm^2, and no radial collimators were used. In Bank 1, the max positive and min negative microstrains appeared at top right and lower left corner of the mapped region, while in Bank 2, they are at lower right and top left corner. Looks like the distribution of them show a mirrored distribution about the Y=0 axis. Bank 6 centered at -65°, which is 25°, off the Bank 1. The lattice *d*-spacing deviation shows slightly higher gradient in Bank 6, while it resembles a distribution profile as in Bank 1. The changes are mostly due to shift of TOF, and because they are from diffraction, the gradient direction follows the scattering vector *Q* direction. As a result, the 0-deviation line is normal to the scattering vector *Q*. That is why the 0-deviation lines in Bank 1 and 2 are perpendicular to each other.

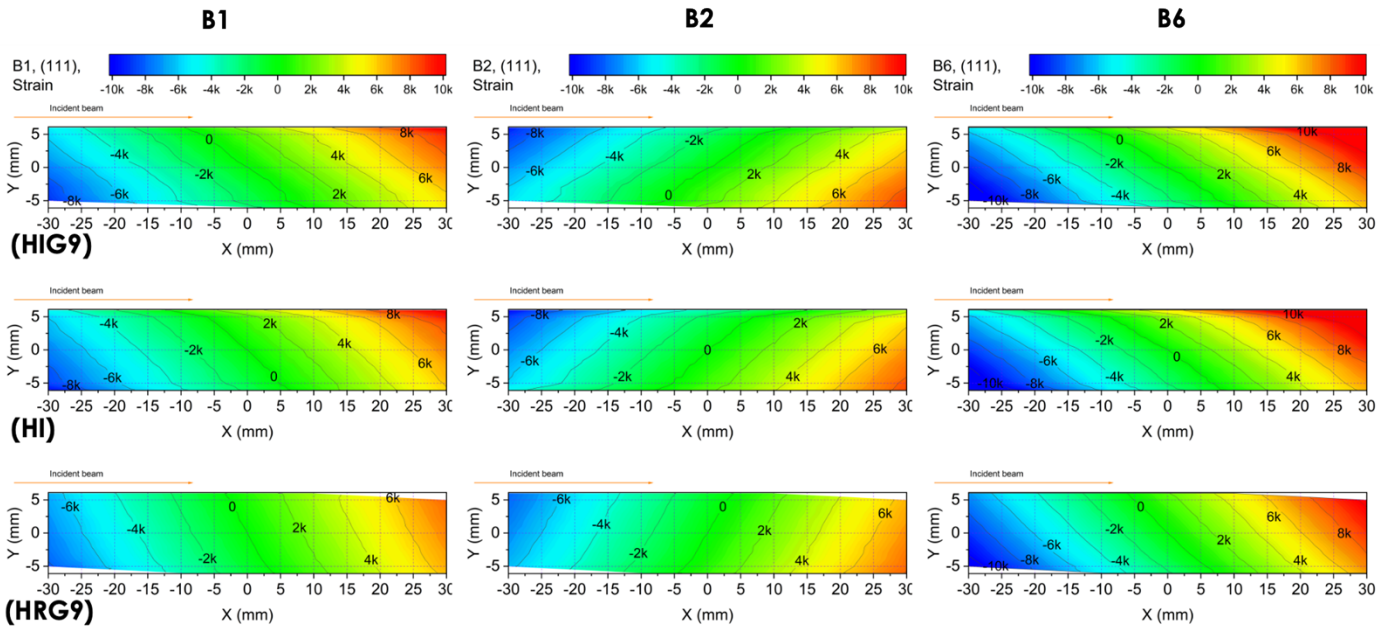

Figure 6. Measured deviation in terms of microstrain of (111) in different banks under different guide settings.

For powder measurements, a 6-mm V can is often used. We zoomed in on Fig. 6 and highlighted a 6-mm-diameter area in the plot, with the circle centered at $X = 0$ mm, $Y = 0$ mm. The zoomed-in plots of (111) are shown in Fig. 7. The lattice deviation in microstrain reaches up to $\pm 1500, \mu\varepsilon$ for Banks 1 and 2, and is higher in Bank 6. Such gradients broaden the peak width. Bank 6 has lower resolution because of its location; the steeper gradient degrades its performance when measuring with a large sample gauge volume. The gradient changes in all three banks exhibit symmetry along their respective Q directions, which cancels the strain shift; therefore, the lattice-spacing measurements are relatively less impacted.

VULCAN is now equipped with high-angle detectors, Bank 3 (120°) and Bank 4 (150°); the position dependence of TOF needs to be investigated. Because (111) cannot be easily measured in all banks due to the different Q coverage of the detector banks, we studied the (311) peaks, which are measured in all detector banks. Similarly, the results of the TOF change expressed in microstrain are shown in Fig. 8. We note that VULCAN measures samples under mechanical loading, and the samples are usually placed horizontally, with the loading-direction strain measured in Bank 1 and the normal direction measured in Bank 2. To assess the impact of the TOF shift on strain measurements under loading, we include a schematic of the horizontal sample area, depicted as a rectangle in Banks 1 and 2. The zoomed-in view of Fig. 8 focusing on the sample areas is shown in Fig. 9. From Figs. 8 and 9, the gradient decreases with increasing scattering angle from downstream to upstream; that is, Bank 6 shows the largest gradient and Bank 4 the smallest. This is expected: TOF shifts arise from changes in the total neutron flight path. For a small displacement Δ along the gradient direction, the change in path length is

$$\Delta L = \frac{2\Delta}{\sin\theta} \quad (2)$$

Therefore, the total path-length change is smaller at larger Q (larger θ). With a rectangular sample gauge area, the spatial heterogeneity of the TOF-change field (in microstrain) differs between banks. On the positive scattering-angle side (Banks 2, 3, and 4), the rectangle's long edge is nearly perpendicular to the gradient, yielding smaller microstrain variation, whereas on the negative scattering-angle side (Banks 1 and 6) it is more aligned with the gradient, yielding larger variation. Consequently, for this sample orientation, Bank 2 performs better than Bank 1, even though their normals have the same offset from the incident beam.

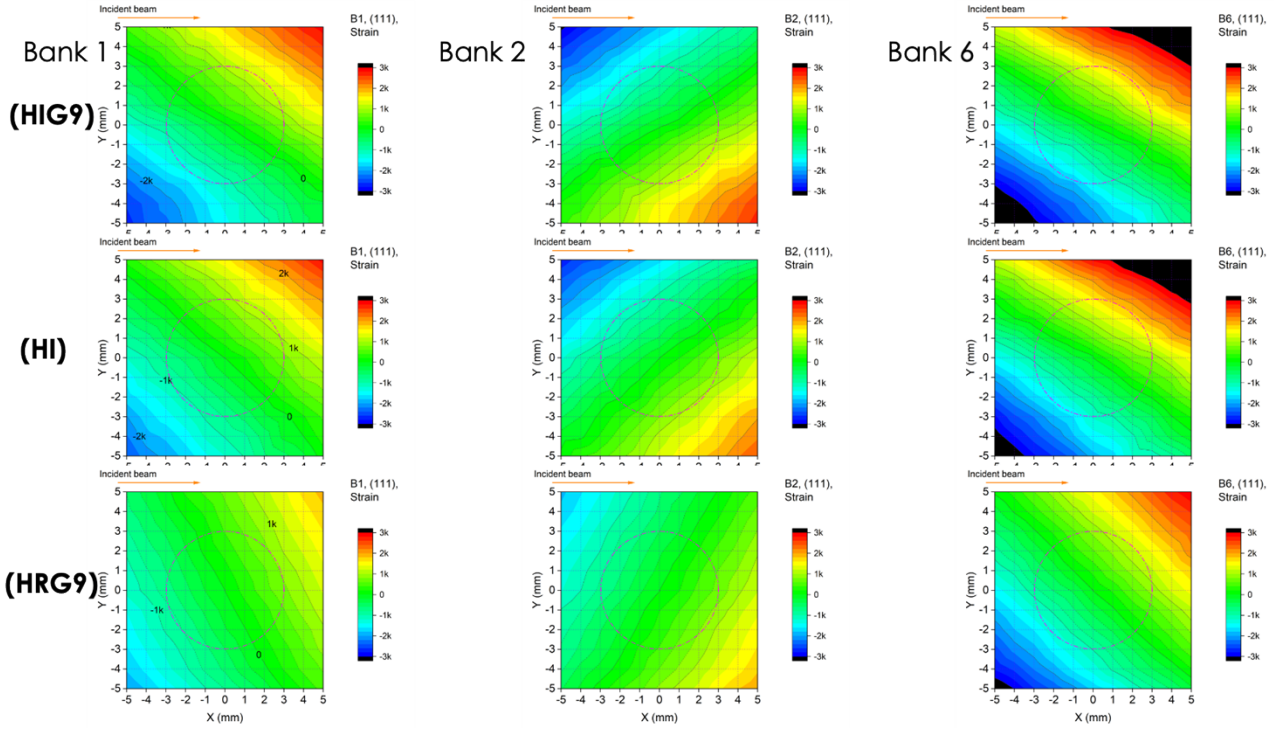

Figure 7. Zoomed-in of Fig. 6 with effective sample area marked.

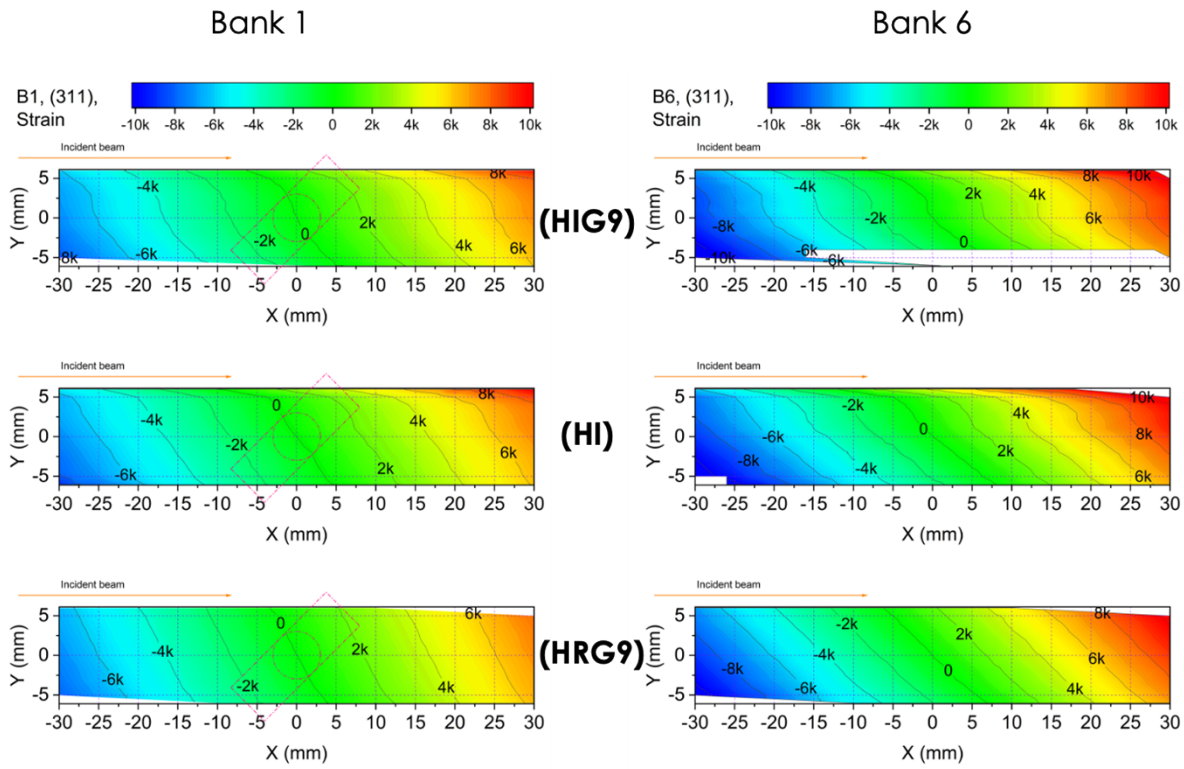

a) Measured deviation in terms of microstrain of (311) in Bank 1 (-90°)and Bank 6 (-65°) on the negative scattering anlge side.

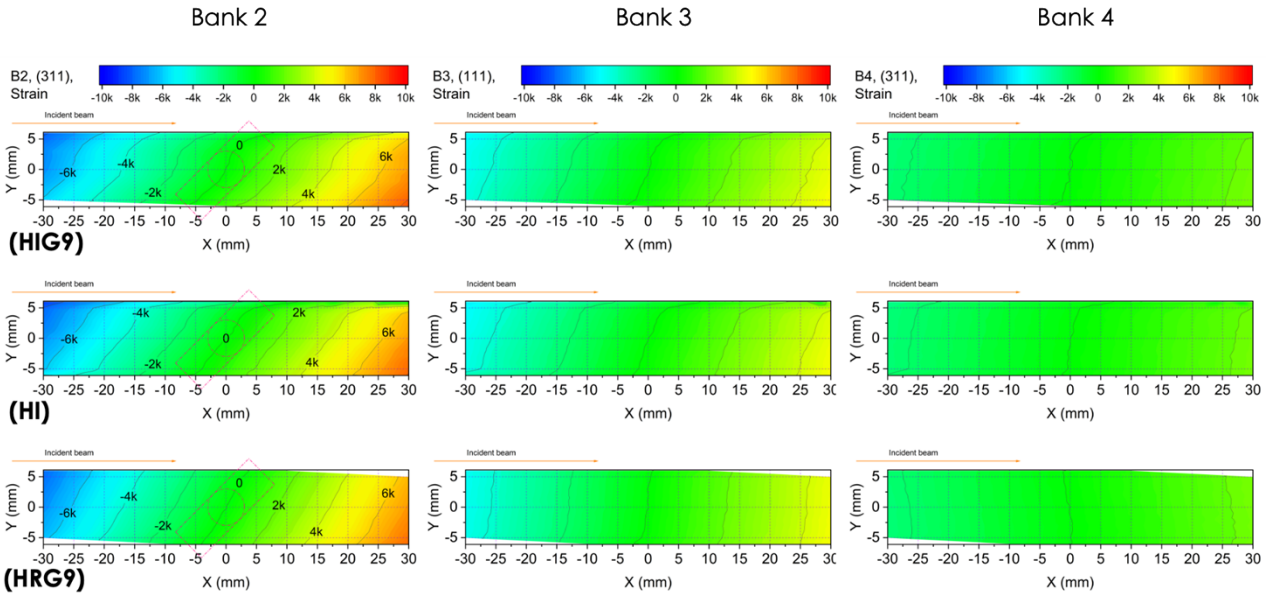

b) Measured deviation in terms of microstrain of (311) in Bank 2 (90°), Bank 3 (120°), and Bank 4 (150°) on the positive scattering angle size.

Figure 8. Measured deviation in terms of microstrain of (311) in different banks under different guide settings.

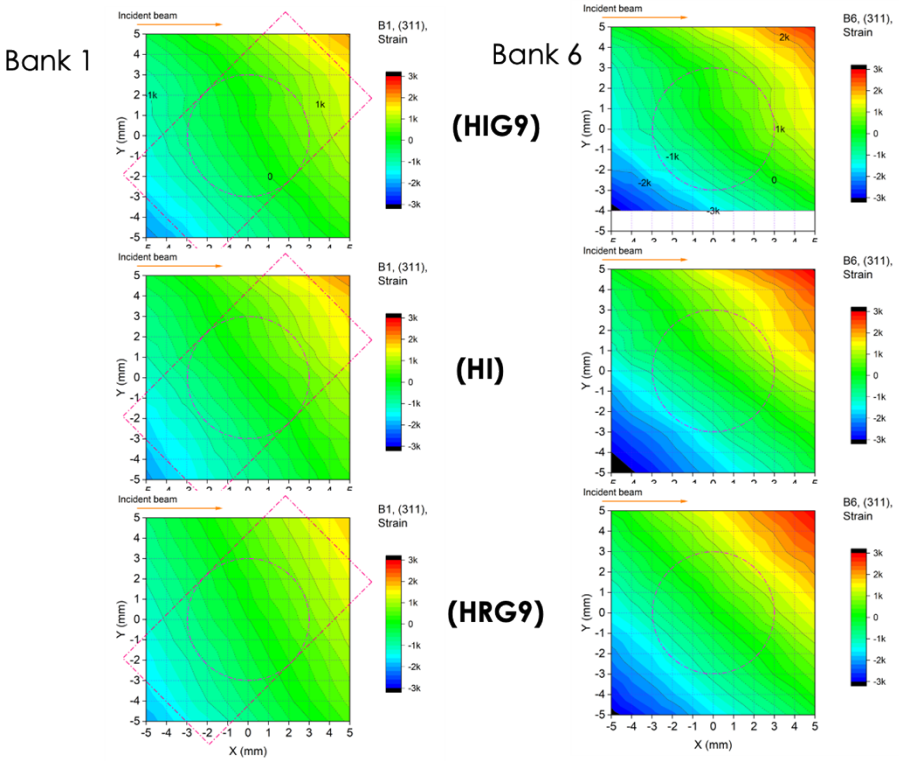

a) Measured deviation in terms of microstrain of (311) in Bank 1 (-90°)and Bank 6 (-65°)on the side of negative scattering anlge.

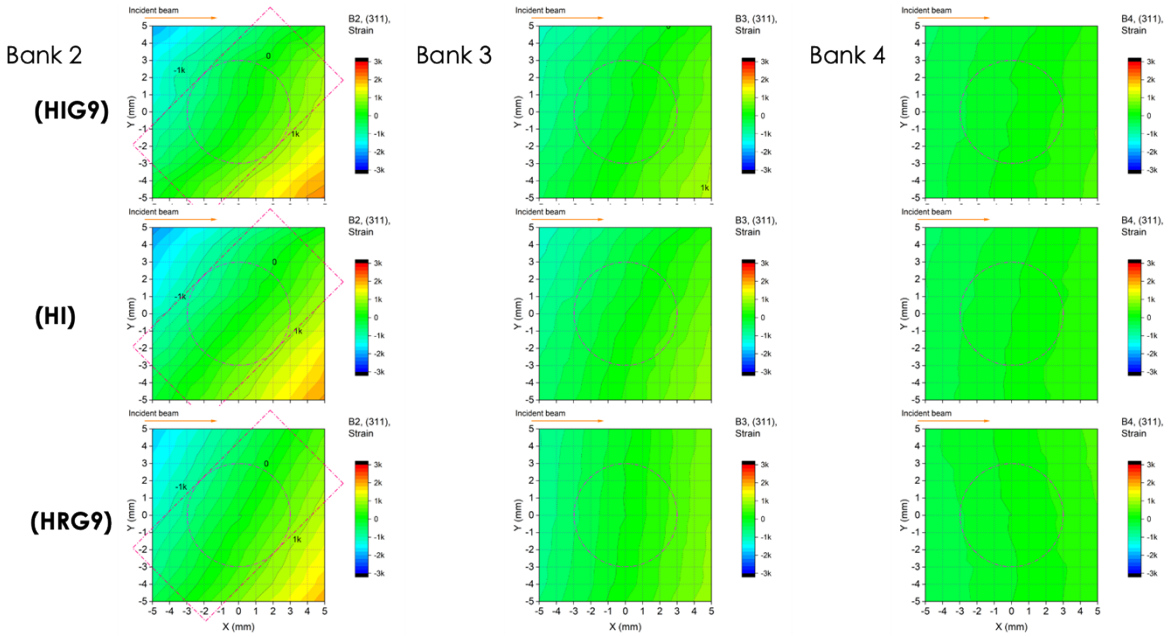

b) Measured deviation in terms of microstrain of (311) in Bank 2 (90°), Bank 3 (120°), and Bank 4 (150°) on the side of positive scattering angle.

Figure 9. Zoomed-in of Fig. 8 with effective sample area marked.

3.3 Measured deviation in X-Y plane from different hkl planes

To investigate the TOF-shift dependence on d-spacing, we analyzed five reflections of diamond powder—(111), (220), (311), (400), and (331)—collected in the representative Bank 1. The results of the lattice deviations in terms of microstrain are shown in Fig. 10. As the lattice d-spacing decreases, the gradient of the microstrain field decreases. With the high-resolution guide setting, the gradient is slightly smaller, and the relative improvement becomes less significant at smaller d-spacings. According to Bragg's law,

$$\lambda=2d\sin(\theta) \quad (3)$$

for a fixed neutron wavelength λ, smaller d-spacings correspond to larger 2θ. From Eq. (2), $\Delta L = 2\Delta/\sin\theta$, so the path-length change—and therefore the TOF-gradient magnitude—is smaller at larger θ, consistent with the observed trend.

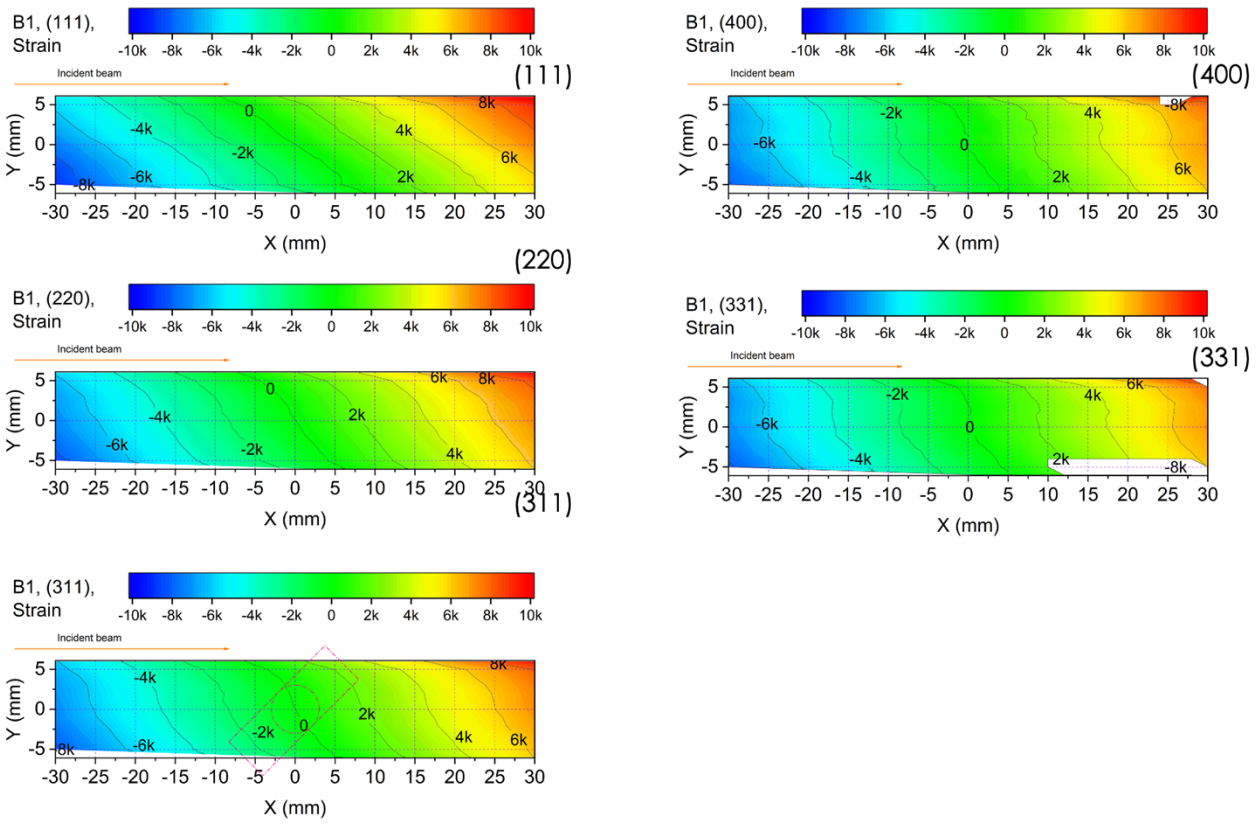

a) Measured deviation in terms of microstrain of the five peaks collected in Bank 1 with HIG9.

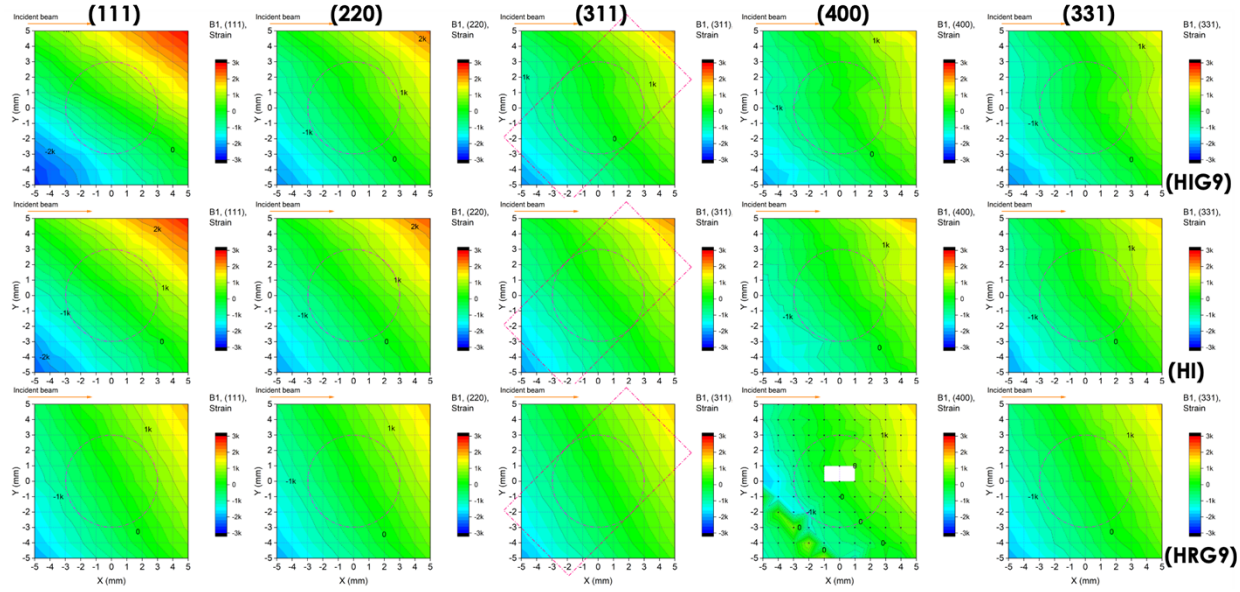

b) Zoomed-in measured deviation in terms of microstrain of the five peaks collected in Bank 1 under the three guide settings.

Figure 10. Tof deviations in terms of microstrain of different hkls in Bank 1.

3.4 Measured deviation in X-Y plane with different horizontal slit openings

Incident slits are often used to confine the beam size for different measurement configurations. We investigated (111) and (311) in Banks 1, 2, and 6 with slit openings of 2 mm, 5 mm, and 12 mm. We show only (311) results for Banks 3, 4, and 5, given the smaller measured Q range of the high-angle detectors. The results are shown in Fig. 11. The beam divergence in the high-intensity modes is larger than in the high-resolution mode; therefore, the beam width at the sample position is better defined in the high-resolution configuration than in the high-intensity mode, with or without the No. 9 guide. Edge effects are observed near the edges of the horizontal opening in the high-intensity modes. Because of the smaller beam size, the edge effect is more pronounced with the 2 mm slit opening.

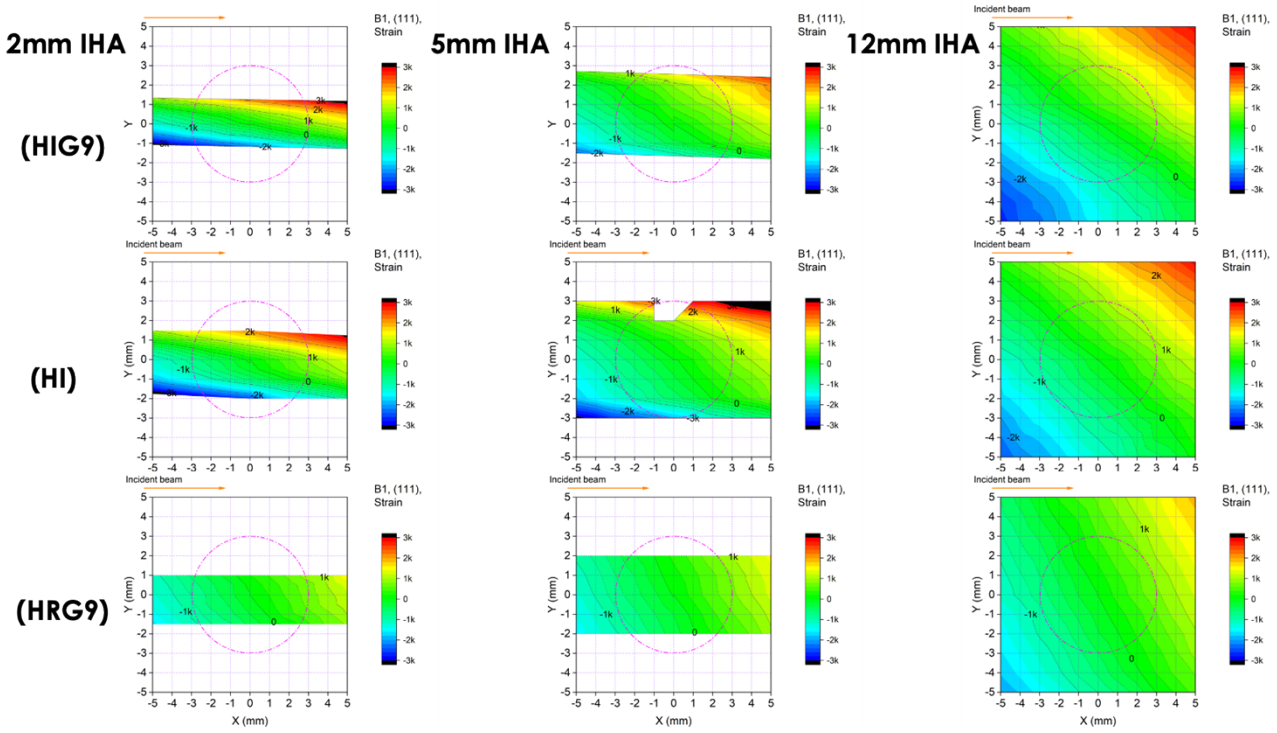

a) Measured deviation in terms of microstrain of (111) measured in Bank 1 with different IHA slit openings.

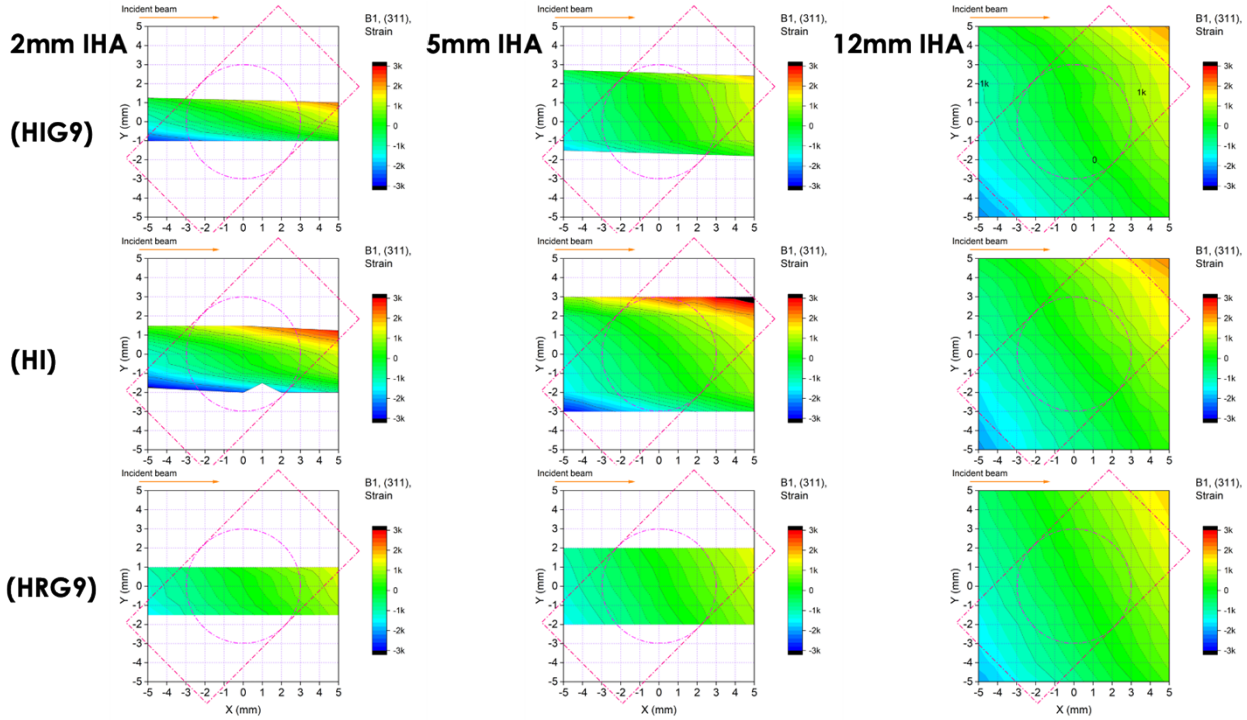

b) Measured deviation in terms of microstrain of (311) measured in Bank 1 with different IHA slit openings.

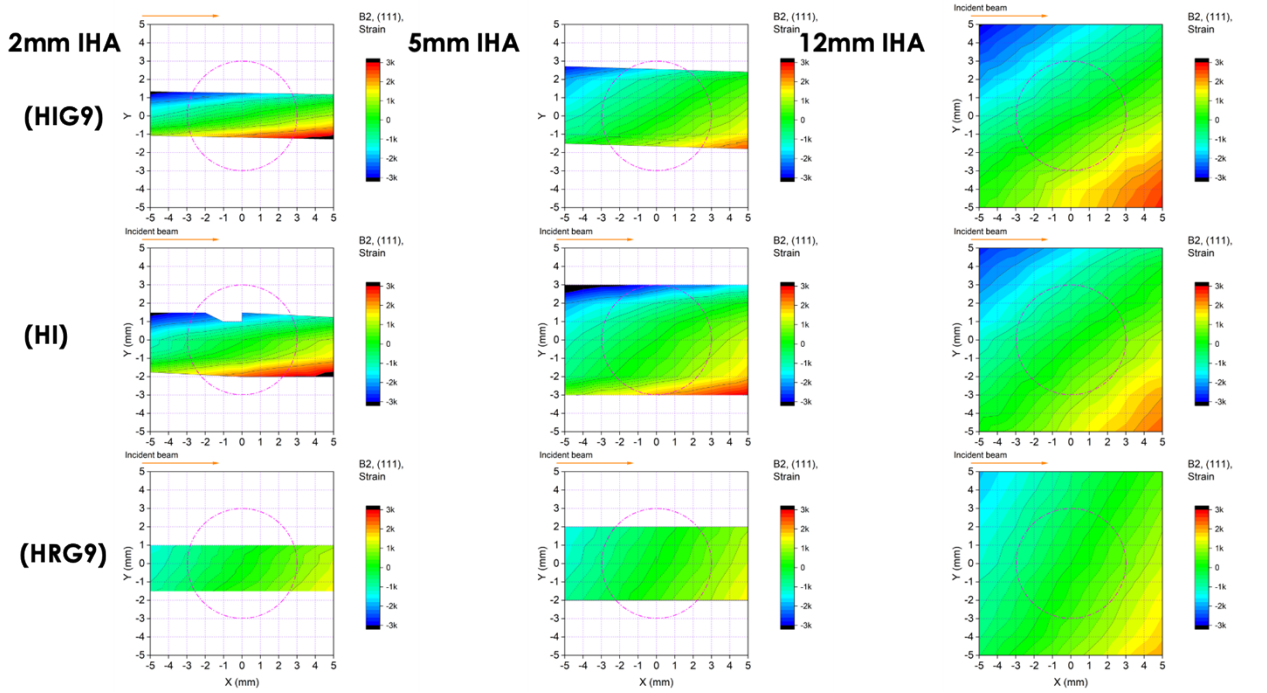

c) Measured deviation in terms of microstrain of (111) measured in Bank 2 with different IHA slit openings.

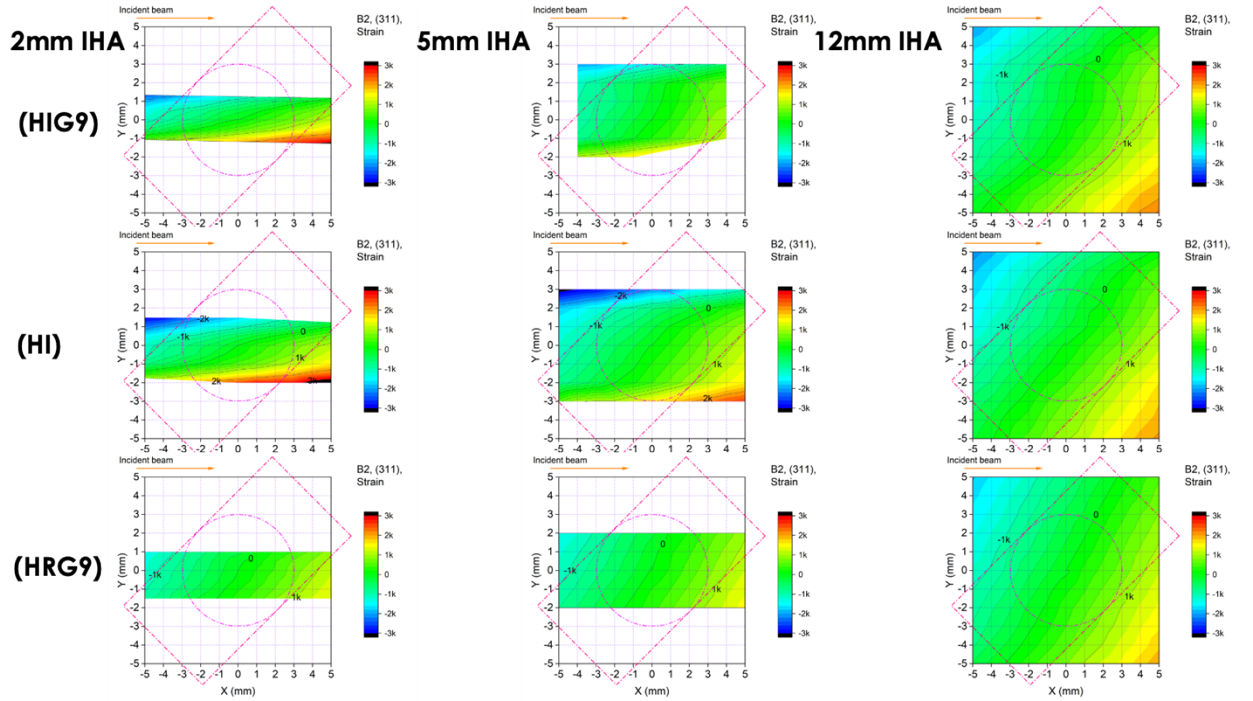

d) Measured deviation in terms of microstrain of (311) measured in Bank 2 with different IHA slit openings.

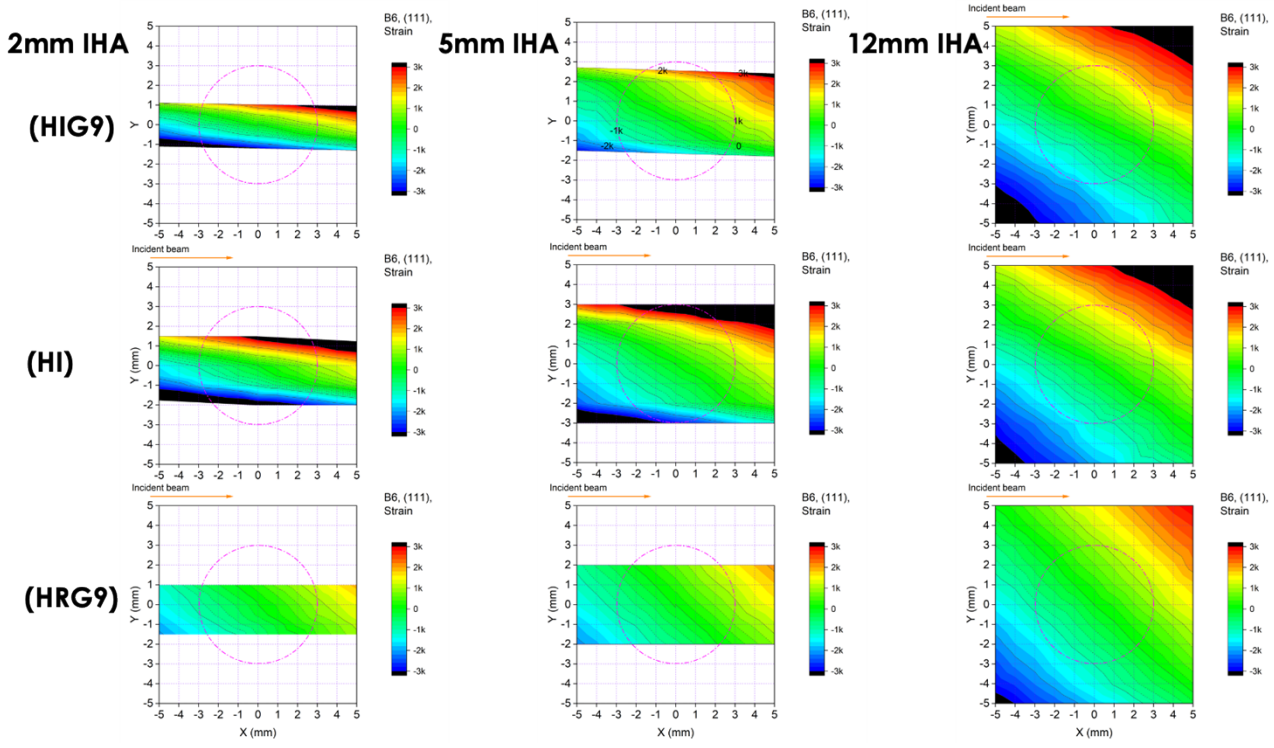

e) Measured deviation in terms of microstrain of (111) measured in Bank 6 with different IHA slit openings.

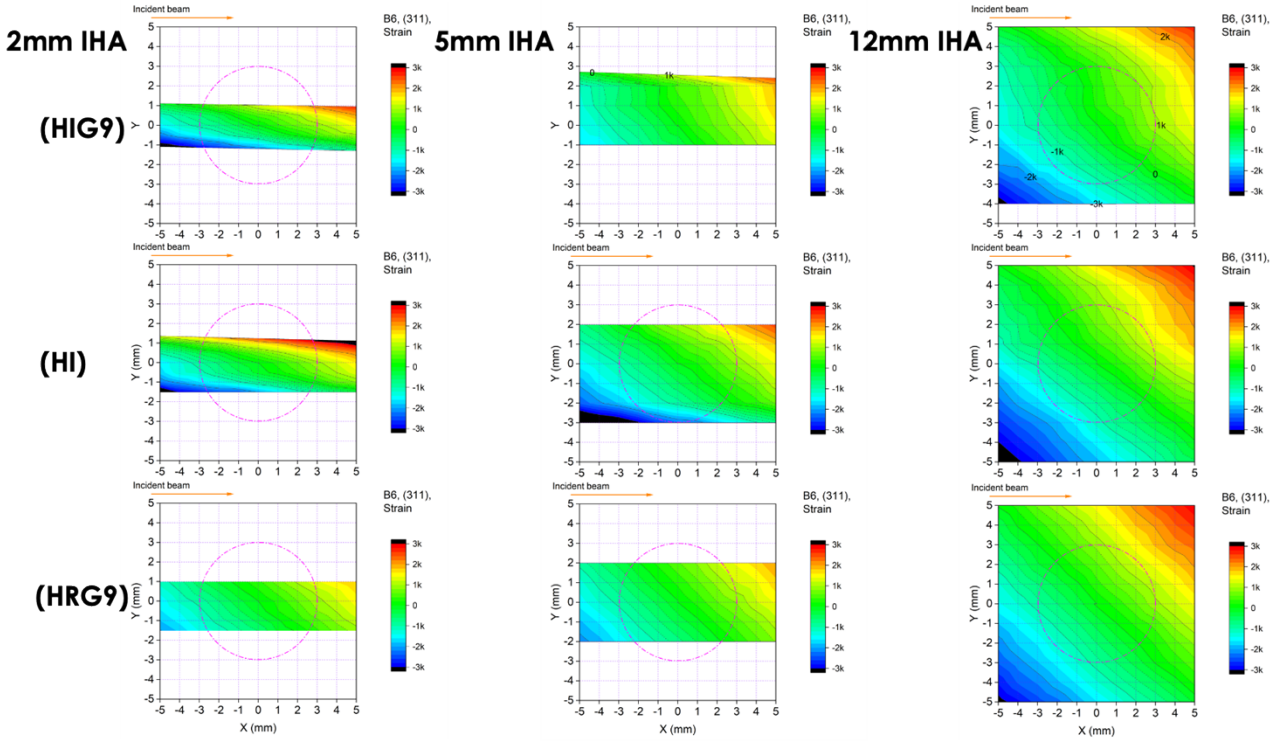

f) Measured deviation in terms of microstrain of (311) measured in Bank 6 with different IHA slit openings.

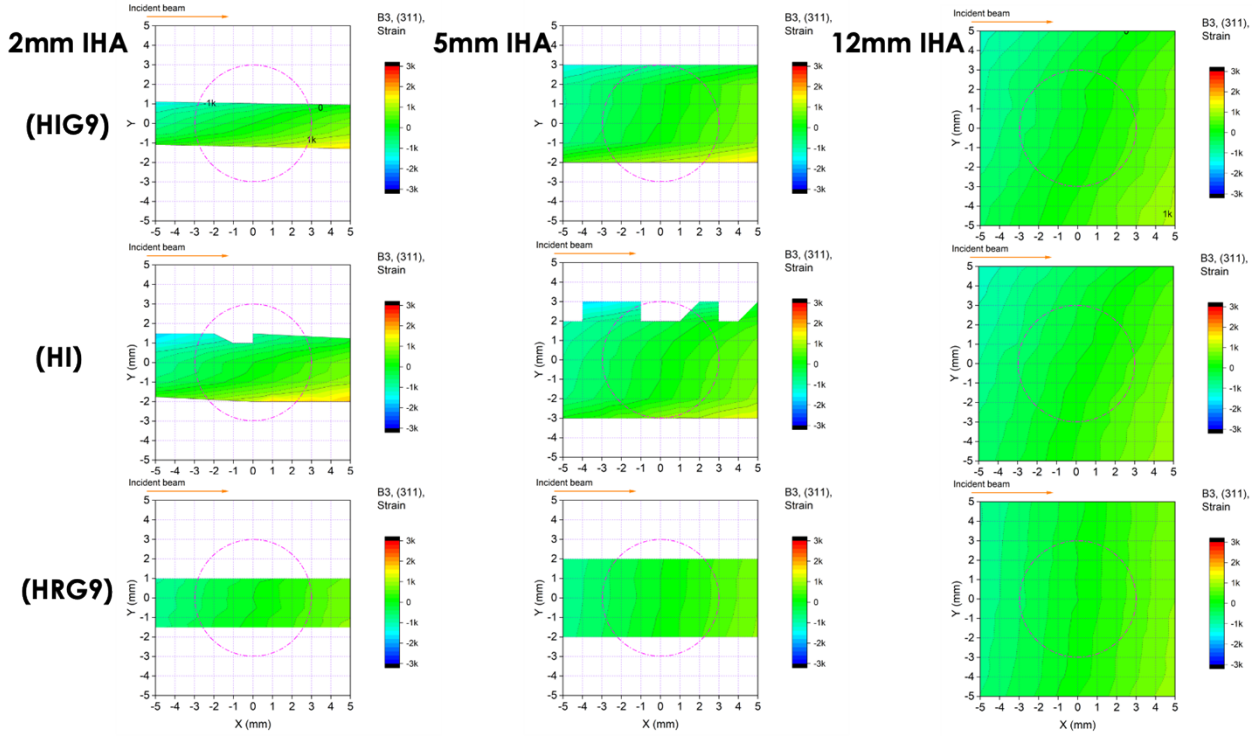

g) Measured deviation in terms of microstrain of (311) measured in Bank 3 with different IHA slit openings.

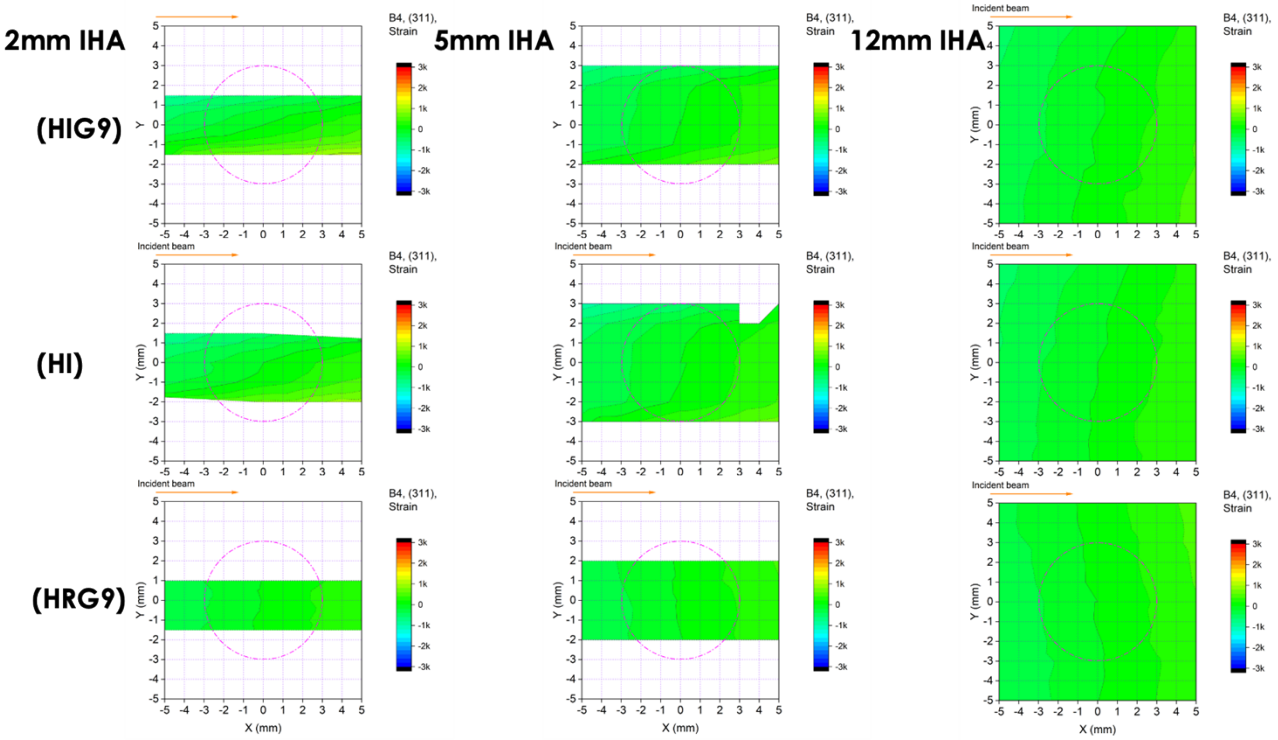

h) Measured deviation in terms of microstrain of (311) measured in Bank 4 with different IHA slit openings.

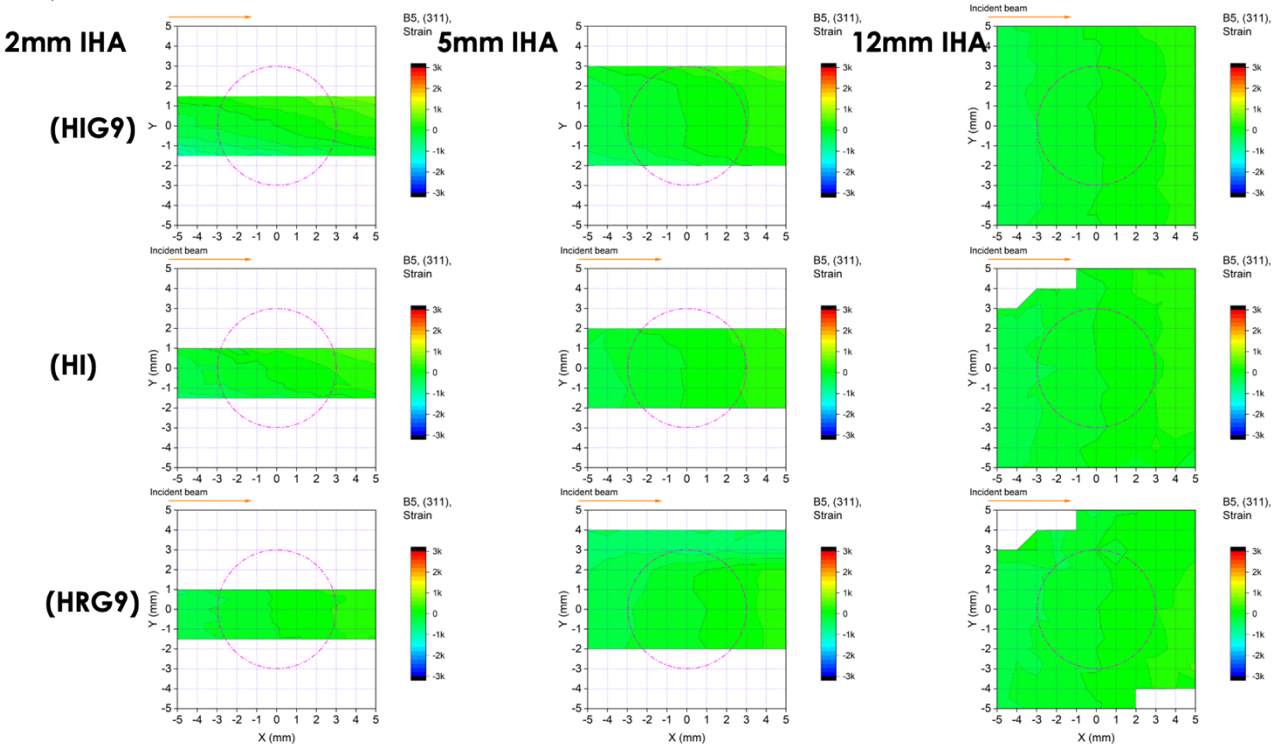

i) Measured deviation in terms of microstrain of (311) measured in Bank 5 with different IHA slit openings.

Figure 11. Deviation in terms of microstrain in X-Y plane with different IHA slit openings.

3.5 Measured deviation in X-Z plane with different horizontal slit openings

To investigate the deviation distribution in the vertical direction, X–Z plane scans were conducted. The diamond powder tube was placed horizontally and translated both vertically and along the beam direction (Z and X, respectively). Two horizontal slit openings were tested: 5 mm and 1 mm. The (311) peak measured in Banks 1–6 is presented, and (111), (220), (311), (400), and (331) in Bank 1 are compared. The results are shown in Fig. 12. Although changes are prominent along the beam direction (X), the variation along Z is within the fitting error. This is expected because no significant change in neutron path length occurs vertically, and any minor vertical path-length differences are canceled out when combining data from individual pixels.

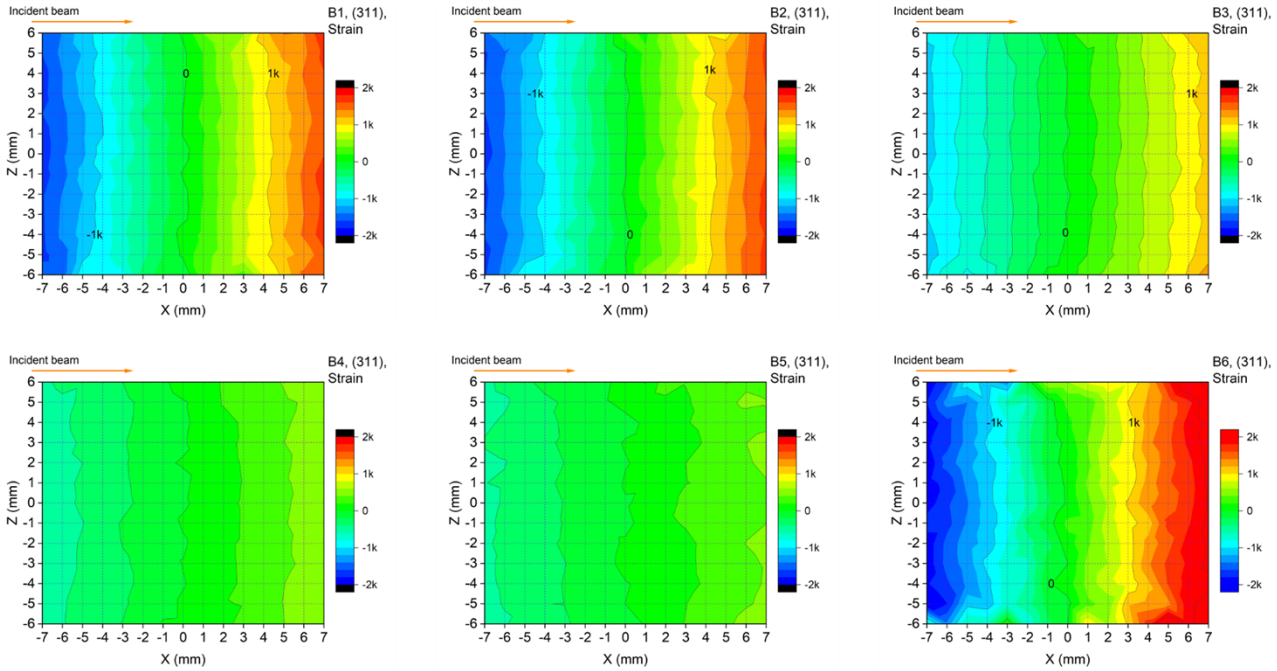

a) Measured deviation in terms of microstrain of (311) in all banks when the IHA slit was opened at 5 mm.

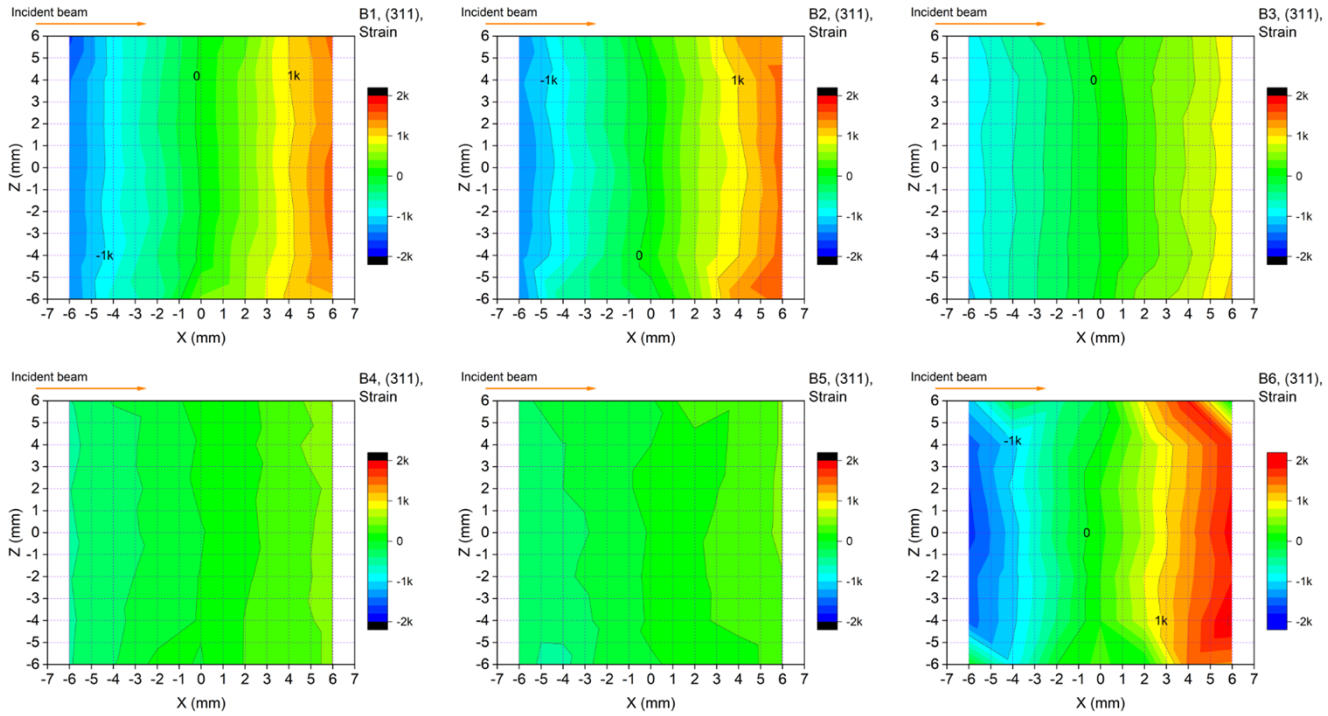

b) Measured deviation in terms of microstrain of (311) in all banks when the IHA slit was opened at 1 mm

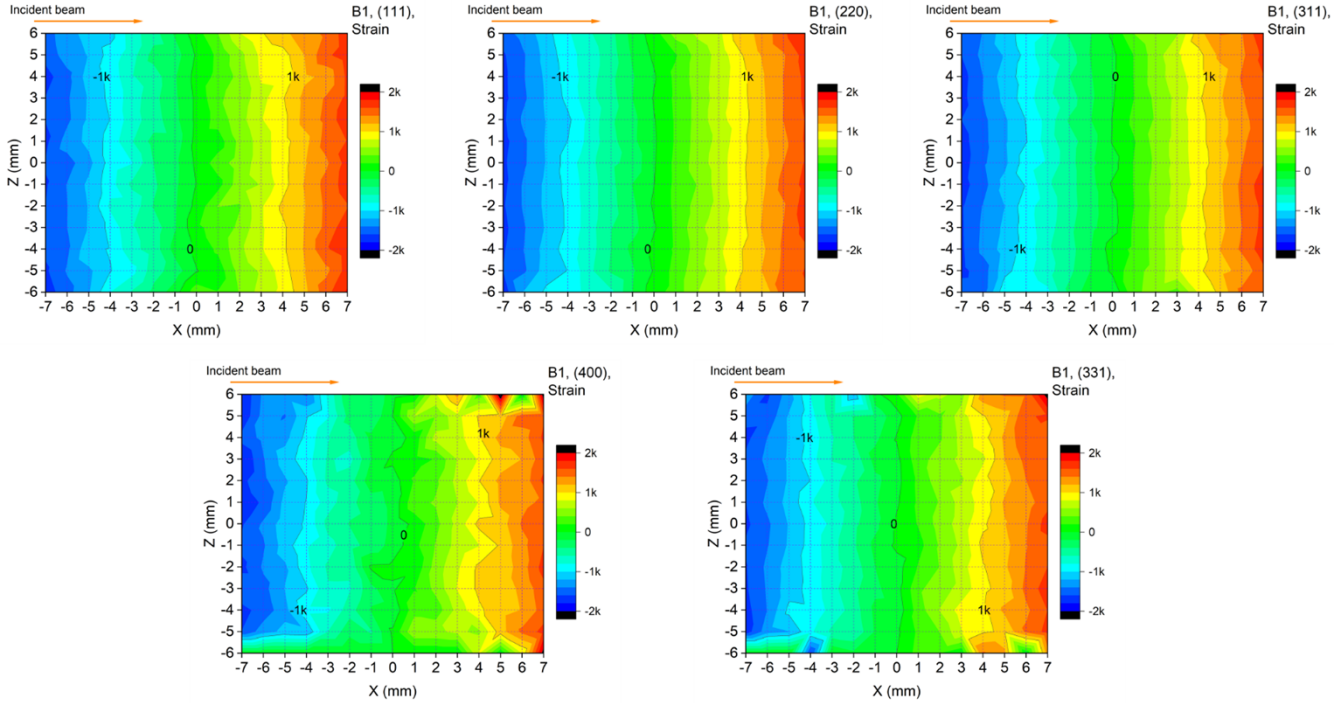

c) Measured deviation in terms of microstrain of (111), (220), (311), (400), and (331) peaks in Bank1 when the IHA slit was opened at 5 mm.

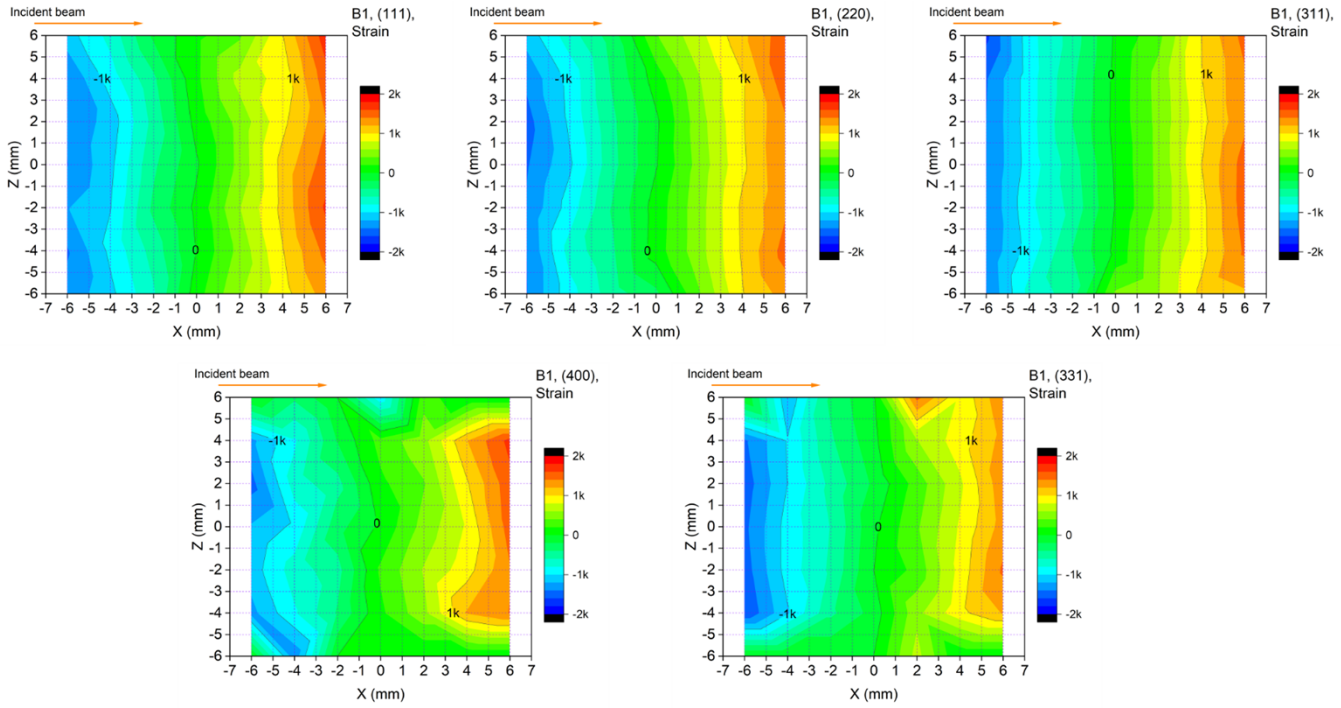

d) Measured deviation in terms of microstrain of (111), (220), (311), (400), and (331) peaks in Bank1 when the IHA slit was opened at 1 mm.

Figure 12. Deviation in terms of microstrain in X-Z plane with different horizonal slit openings.

4. Summary

At a TOF diffractometer, many factors can lead to shifts in TOF values. In this report, we present a detailed analysis of the relative TOF deviation expressed in microstrain by scanning the beam coverage with a 1-mm diamond powder sample under different instrument configurations. The shift in TOF or in the measured d-spacing arises from changes in neutron flight path, which depend on sample position, neutron guide optics, detector location, and Bragg scattering angle. An edge effect is also observed and has a greater impact when using smaller slit sizes than larger slits. We identified the affected areas by marking two typical use cases: powder measurements and mechanical-loading experiments. Because of symmetry, the effect on lattice spacing is minimized, but peak broadening is affected.

REFERENCE

[1] K. An, H. D. Skorpenske, A. D. Stoica, D. Ma, X.-L. Wang, and E. Cakmak, "First In Situ Lattice Strains Measurements Under Load at VULCAN," *Metall. Mater. Trans. A*, vol. 42, no. 1, pp. 95–99, Jan. 2011, doi: 10.1007/s11661-010-0495-9.

[2] K. An, Y. Chen, and A. D. Stoica, "VULCAN: A 'hammer' for high-temperature materials research," *Mrs Bull.*, vol. 44, no. 11, pp. 878–885, 2019.

[3] E. B. Iverson, A. D. Stoica, and W. Lu, "Intensity Gain from VULCAN Guide 9," Oak Ridge National Laboratory, Oak Ridge, Technical Memo 106100200-TR0202-R00, Oct. 2013.

[4] K. An, "VDRIVE-Data reduction and interactive visualization software for event mode neutron diffraction," *ORNL Rep. No ORNL-TM-2012-621*, vol. 18, 2012.

[5] A. C. Larson and R. B. Von Dreele, "General Structure Analysis System (GSAS)," Los Alamos National Laboratory, LAUR 86-748, 2004.

ACKNOWLEDGEMENT

This research used resources at the Spallation Neutron Source, a DOE Office of Science User Facility operated by the Oak Ridge National Laboratory. The beam time was allocated to VULCAN on proposal number IPTS-30088, IPTS-31653.

This page is intentionally left blank.